Available online at www.sciencedirect.com
SCIENCE DIRECT
Journal of Solid State Chemistry 179 (2006) 2714–2720
JOURNAL OF SOLID STATE CHEMISTRY
www.elsevier.com/locate/jssc

Electron-irradiation induced phase transformation in $La_{1/3}Zr_2(PO_4)_3$: La^{3+} displacement in a preserved NASICON framework

M.P. Crosnier-Lopez*, M. Barre, F. Le Berre, J.L. Fourquet

Laboratoire des Oxydes et Fluorures (UMR CNRS 6010), Institut de Recherche en Ingénierie Moléculaire et Matériaux Fonctionnels (FR CNRS 2575), Faculté des Sciences et Techniques, Université du Maine, Av. O. Messiaen, 72085 Le Mans Cedex 9, France

Received 17 February 2006; received in revised form 10 April 2006; accepted 20 May 2006
Available online 3 June 2006

Abstract

The $La_{1/3}Zr_2(PO_4)_3$ NASICON-type compound (S.G. $P\bar{3}$ - neutron and X-ray diffraction experiments) is investigated by transmission electron microscopy (TEM) technique, selected area electron diffraction (SAED) and high-resolution electron microscopy (HREM), in order to study locally the lanthanum distribution. An irreversible structural transformation (P - - - $\rightarrow$ P - c - $\rightarrow$ R - - -) is observed, without modification of the atomic content and cell size, as soon as the phase is illuminated by the electron beam. The progressive disappearance of the spots which do not check the R conditions on the SAED patterns is clearly shown along two zone axis, [001] and [100]. This transformation implies the displacement of the two La^{3+} cations in a preserved classical $[Zr_2(PO_4)_3]^-$ network. This interesting behavior is in good agreement with the La^{3+} ionic conductivity observed in $La_{1/3}Zr_2(PO_4)_3$ (4.09×10^{-7} S cm^{-1} at 700 °C). To our knowledge, this is the first time that a complete TEM study is done on a NASICON-type phase.

Keywords: NASICON-type phase; Transmission electron microscopy; Electron-induced structural change; Lanthanum displacement; $La_{1/3}Zr_2(PO_4)_3$

1. Introduction

Many related zirconium phosphates [1] have been considerably studied since the work of Sljukic et al. [2] in 1967 on $NaZr_2(PO_4)_3$. In this family, the $RE_{1/3}Zr_2(PO_4)_3$ series, which are found to be trivalent cationic solid electrolytes [3], has not been well structurally characterized. Recently, we published the structure [4] of $La_{1/3}Zr_2(PO_4)_3$ with a new space group -$P\bar{3}$- for a NASICON-type compound. Indeed, X-ray powder and neutron diffraction demonstrated that the rhombohedral space groups $R\bar{3}$ and $R\bar{3}c$ usually encountered in this family of materials are excluded due to the presence of (002), (004) and (101) diffraction peaks at low 2θ angle. In this compound, the $[Zr_2(PO_4)_3]^-$ network is preserved and the two La^{3+} ions are found quasi-ordered along the c-axis, mainly distributed on the two sites, 1a and 1b. However, a NMR study (^{31}P MAS and 2D DQ experiments) allows to reveal that the sample is constituted by two kinds of domains: one corresponding to the perfect ordering of the La^{3+} ions on the La1 and La2 positions (1a and 1b sites in $P\bar{3}$ space group); the other, presenting some extra La^{3+} ions distributed on the La3 position (2d site in the $P\bar{3}$ space group). The structure obtained by powder diffraction study can then be considered as an average structure. In order to confirm the local lanthanum distribution, we have undertaken a complete TEM study, selected area electron diffraction (SAED) and high-resolution electron microscopy (HREM), on $La_{1/3}Zr_2(PO_4)_3$ which has revealed an interesting behavior. Oddly, to our knowledge, this is the first time that a NASICON-type compound is studied by TEM technique.

2. Experimental

2.1. Synthesis and structural characterization

$La_{1/3}Zr_2(PO_4)_3$ powder is synthesized by the Pechini sol–gel method [5] from La_2O_3, $ZrOCl_2 \cdot 8H_2O$ and $NH_4H_2PO_4$ in stoechiometric ratios as described in [4].

*Corresponding author. Fax: +33 2 43 83 35 06.
E-mail address: marie-pierre.crosnier-lopez@univ-lemans.fr (M.P. Crosnier-Lopez).

0022-4596/$ - see front matter © 2006 Elsevier Inc. All rights reserved.
doi:10.1016/j.jssc.2006.05.031

The structure is determined from both X-ray and neutron powder diffraction data [4].

2.2. Transmission electron microscopy (TEM)

The TEM studies, SAED and HREM, are carried out with a JEOL 2010 electron microscope operating at 200 kV and equipped with a side entry $\pm 30^\circ$ double-tilt specimen holder. EDX analysis is done on crystallites with a KEVEX energy-dispersive X-ray spectrometer coupled with the TEM. Simulations are performed with the JEMS program (electron microscopy software - java version 2.081W2005) of Stadelman [6] with the multislice formalism. Images are computed for different thickness and defocus values using the following microscope parameters: spherical aberration constant $Cs = 1$ mm, defocus spread $\Delta = 12$ nm, semi-convergence angle $\alpha = 1.4$ mrad and objective aperture diameter 11.6 nm^{-1}. The sample chosen for this study is the one used for the structural determination: a small part of sieved sample is put in *n*-butanol and ultrasonically dispersed, with no additional crushing in order to preserve the sample structure. A drop of the resulting suspension is deposited on the holey carbon film of a Cu grid, leaving crystallites in random orientation after drying.

3. Results and discussion

3.1. Description of the structure

The room temperature (RT) structure of $La_{1/3}Zr_2(PO_4)_3$ can be described in the $P\bar{3}$ space group [4] from the classical $[Zr_2(PO_4)_3]^-$ NASICON-type network (Fig. 1a) in which four sites - all in a six-fold coordination antiprism LaO_6 - are available for the two La^{3+} ions: 1*a* (0, 0, 0) (La1), 1*b* (0, 0, 1/2) (La2) and two 2*d* sites (1/3, 2/3, *z*) with $z \sim 2/3$ (La3-2*d* site) and $2/3 + 1/2$ (La4-2*d*′ site). However, structural refinements reveal that the fourth site is empty, and that the two La^{3+} ions are mainly located on the 1*a* and 1*b* sites leading to a quasiordered situation along the *c*-axis: one La^{3+} on the 1*a* (0, 0, 0) and 0.82 La^{3+} on the 1*b* (0, 0, 1/2) sites, the remaining 0.18 La^{3+} ions occupying partially a 2*d* site (1/3, 2/3, 0.667(5)). The La^{3+} ions exhibit high isotropic temperature factor (7.2 $Å^2$ from neutron data) which can be associated with quite large La–O distances (2.47–2.60 Å) compared to the sum of the ionic radii [7] (2.38 Å). Low bond valence sums [8] for La^{3+} ions (1.90, 2.70 and 1.11, respectively for La1, La2 and La3) are consequently obtained. This structural fact is in good agreement with the RE^{3+} ionic conductivity observed in such compounds [3]. By comparison, in $La_{1/3}Ti_2(PO_4)_3$ [9], the bond valence sum of the La^{3+} ions located in the 3*a* site can be calculated equal to 2.33 with six equal distances La–O close to 2.52 Å.

3.2. TEM study

All the particles observed are small (< 100 nm) and well crystallized with most often rounded irregular shape (no faceted borders). As expected, the reciprocal space reconstitutions by SAED technique, carried out with a great number of crystallites, always lead to the classical NASICON hexagonal cell ($a \approx 8.7$ and $c \approx 23.2$ Å). However, extinction conditions inconsistent with the $P\bar{3}$ space group previously announced, are systematically present leading to propose an *R*– – – extinction symbol. A careful examination of the patterns during illumination reveals an evolution of the spots intensity. In such conditions, additional reconstitutions are tested with less irradiation

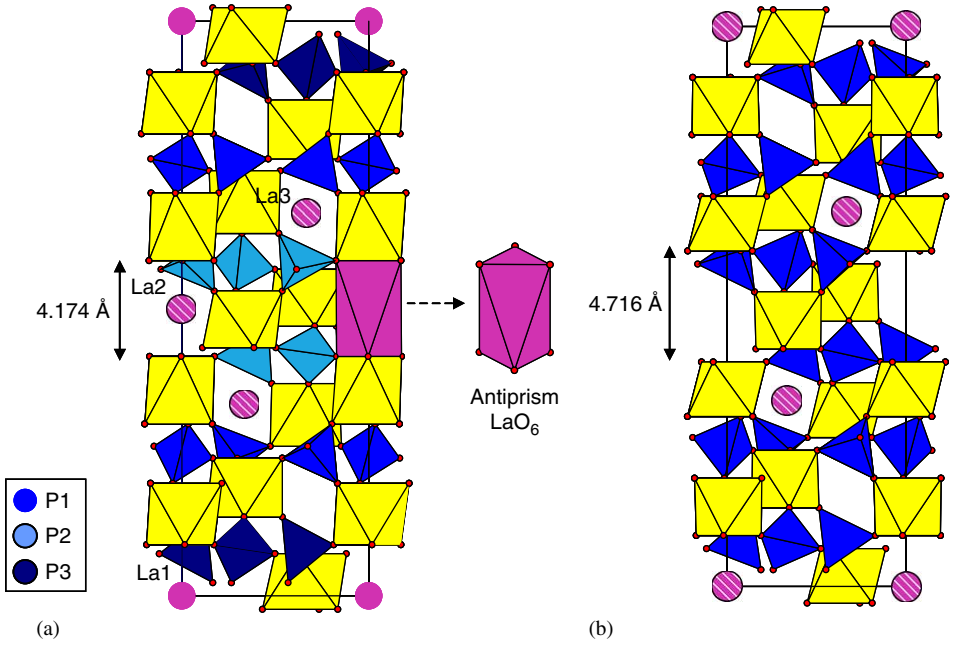

Fig. 1. Projection of the structures of $La_{1/3}Zr_2(PO_4)_3$ (a) and $La_{1/3}Ti_2(PO_4)_3$ (b) along the *b*-axis (hatched La circles represent partially occupied sites).

of the specimen ($\approx 8\,pA.cm^{-2}$ at a magnification of 80×10^3 instead of the value $30\,pA.cm^{-2}$ classically used) and reveal a transformation of the SAED patterns during observation. Unfortunately, despite our efforts and the low intensity of the electron beam, this transformation is too fast to allow us to do a reconstitution of the reciprocal space of the $P\bar{3}$ form: we just succeeded in making several patterns on different particles during the transformation (Figs. 2 and 3). On Fig. 2, corresponding to the [001] zone axis (ZA), we can see a progressive disappearance of the spots which do not check the R conditions ($-h+k+l=3n$) while the intensity of the others seems unmodified. As an example, the white arrows allow to see the transformation of an $h\,k\,l$ spot forbidden in an R mode: its intensity is strongly affected during the four steps presented. Similarly, the transformation can be followed along the [100] ZA on Fig. 3, where three successive steps are proposed. The first one, Fig. 3a, obtained at the beginning of the transformation, shows new unexpected condition ($h\,0\,l$, $l=2n$) corresponding to a c plane and leading to a possible extinction symbol P - c -, in dissension with the RT X-ray results (S.G. $P\bar{3}$). At the end of the transformation (Fig. 3c), an R condition is revealed as for the [001] ZA. Between these two steps, we observe an intermediate situation where the both forms (P - c - and R– – –) coexist (Fig. 3b). It can be evidenced by digitalizing together the two patterns 3a and 3c: the result obtained (Fig. 3a + c) is in excellent correlation with the intermediate situation of Fig. 3b, leading to a particular extinction condition along the c^* axis (shown by the circles).

During the transformation, the cell size remains unchanged since the reciprocal space reconstitutions of the final form give a NASICON-type cell and the spots corresponding to an R mode can be perfectly superposed. This implies then the preservation of the $[Zr_2(PO_4)_3]^-$ network. It can be noted that such a process seems to be irreversible: a crystallite exposed and showing an R mode does not reveal an inverse transformation even after 1 week. Moreover, this transformation occurs without modification of the atomic content: an EDX analysis performed at the beginning and at the end of the observation confirms the presence of O, La, Zr and P with preserved ratios.

The unexpected conditions revealed at the beginning of the transformation ($h\,0\,l$, $l=2n$) lead to two space groups: the acentric one $P3c1$ (no. 158) and the centric $P\bar{3}c1$ (no. 165). Although these groups are never used until now to describe NASICON-type compounds, this situation is not surprising since all the atomic coordinates can be easily transposed from the usual $R\bar{3}$ space group to $P\bar{3}c1$. However, this first form observed in the TEM study of $La_{1/3}Zr_2(PO_4)_3$ is then not the original form ($P\bar{3}$), which carries us to believe that this compound transforms as soon as it is illuminated by the electron beam.

A careful examination of the $[Zr_2(PO_4)_3]^-$ network in the original $P\bar{3}$ form of $La_{1/3}Zr_2(PO_4)_3$ shows that the atomic positions are not far from a R symmetry. The main difference between the description in the three groups $P\bar{3}$, $P\bar{3}c1$ and $R\bar{3}$ concerns the La^{3+} distribution in the $[Zr_2(PO_4)_3]^-$ network (Table 1 and Fig. 4): in the $P\bar{3}$ space group, four sites (1a, 1b, 2d and 2d') are available; in the $P\bar{3}c1$, only two sites exist (2b and 4d, the site 2b corresponding to the sites 1a and 1b of $P\bar{3}$, while the 4d sites are correlated with the 2d and 2d' sites of $P\bar{3}$); finally, in the $R\bar{3}$ space group, the two available positions are 3a (1a and 2d in $P\bar{3}$) and 3b (1b and 2d' in $P\bar{3}$). In such conditions, TEM observations imply La^{3+} displacements in a preserved network obtained by a small and concerted motion of all the others atoms (Zr, P and O). These La^{3+} displacements can be correlated with the ionic conductivity property [3] observed for this NASICON-type phase.

In order to complete the description of this observed transformation, we undertake an HREM study along the a direction, which allows to separate the available La^{3+} sites as one can see on the Fig. 4. In a first time, we note during a lot of HREM tests that the observed crystallite systematically loses slowly its orientation with a continuously tilting while a progressive amorphisation of the thinnest part of the crystal occurs, giving thus poor-quality photographs. However, despite this problem, we succeeded to make one HREM image as one can see in Fig. 5a: two different contrast zones can be seen in the circles, while the

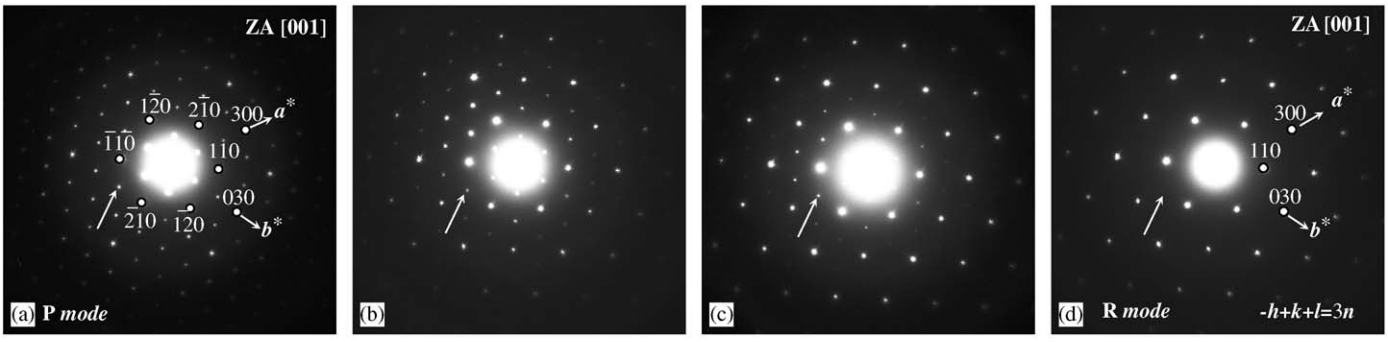

Fig. 2. SAED patterns of a crystallite of $La_{1/3}Zr_2(PO_4)_3$ at the beginning of the observation (a), during (b and c) and after (d) the transformation P - c - → R - - - in the [001] ZA; The white arrows show the progressive vanishing of one $h\,k\,l$ spot forbidden in an R mode.

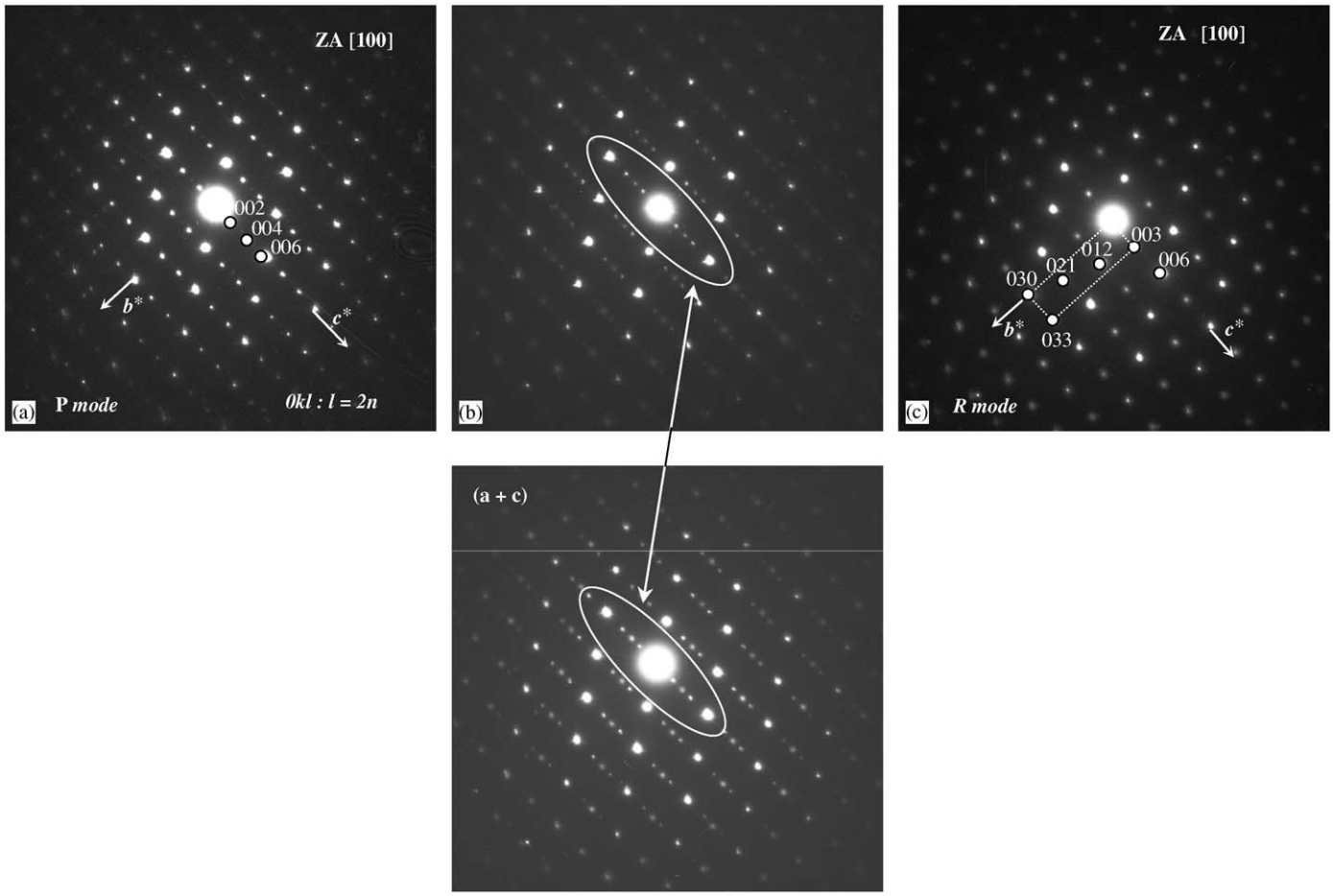

Fig. 3. SAED patterns of a crystallite of $La_{1/3}Zr_2(PO_4)_3$ at the beginning of the observation (a), during (b) and after (c) the transformation P - c - $\rightarrow R$ - - - in the [100] ZA. The intermediate step (b) can be considered as a coexistence of both forms (P - c - $\rightarrow R$ - - -) as a similar pattern ($a+c$) can be obtain by digitalizing together the two steps (a) and (c).

Table 1
$La_{1/3}Zr_2(PO4)3$:$P\bar{3} \rightarrow P\bar{3}c1 \rightarrow R\bar{3}$: transposition of atomic positions

Atom type	$P\bar{3}$ (no. 147)[a]	$P\bar{3}c1$ (no. 165)	$R\bar{3}$ (no. 148)[b]
La	1a,(0, 0, 0) 1b, (0, 0, 1/2) $2\times 2d$, (1/3, 2/3, z): $z\approx$ 2/3(2d) and 2/3+1/2(2d')	2b, (0, 0, 0) 4d, (1/3, 2/3, z): $z\approx$ 2/3	3a, (0, 0, 0) 3b, (0, 0, 1/2)
Zr	$2\times 2c$, (0, 0, z): $z\approx$0.14 and 0.65 $4\times 2d$ (1/3, 2/3, z): $z\approx$0.02, 0.31, 0.53 and 0.80	4c, (0, 0, z): $z\approx$0.14 4d, (1/3, 2/3, z): $z\approx$0.81 4d, (1/3, 2/3, z): $z\approx$0.53	$2\times 6c$, (0, 0, z): z = 0.1469 and 0.6424
P	$3\times 6g$, (x, y, z): 0.28, 0.99, 0.25 0.95, 0.33, 0.58 0.62, 0.66, 0.92	6f, (x, 0, 1/4): $x\approx$0.28 12g, (x, y, z):0.95, 0.33, 0.58	18f, (x, y, z): 0.2854, 0.0047, 0.2517
O	$12\times 6g$, (x, y, z)	$6\times 12g$, (x, y, z)	$4\times 18f$, (x, y, z)

[a]$La_{1/3}Zr_2(PO_4)_3$ in the original form crystallizes in the $P\bar{3}$ space group.
[b]The atomic coordinates are related to $La_{1/3}Ti_2(PO_4)_3$ [9] at 25 °C: in this compound, La^{3+} ions are only located in the site 3a with a 2/3 occupancy factor.

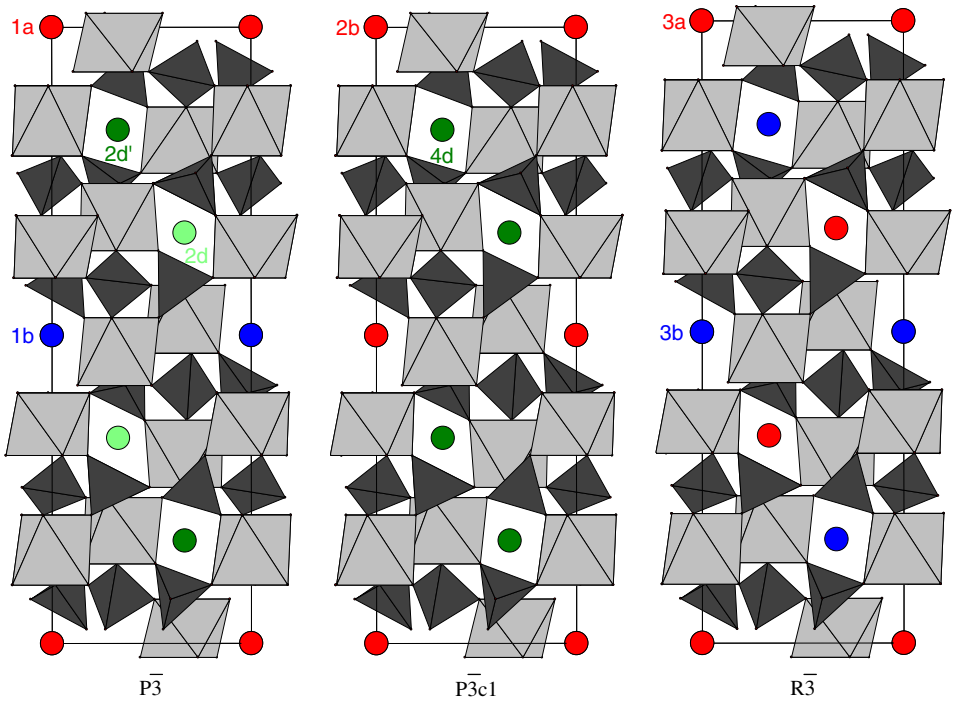

Fig. 4. Projection of the NASICON-type structure in the three space group $P\bar{3}$, $P\bar{3}c1$ and $R\bar{3}$ showing the different sites available for the two La^{3+} cations in a preserved $[Zr_2(PO_4)_3]^-$ framework.

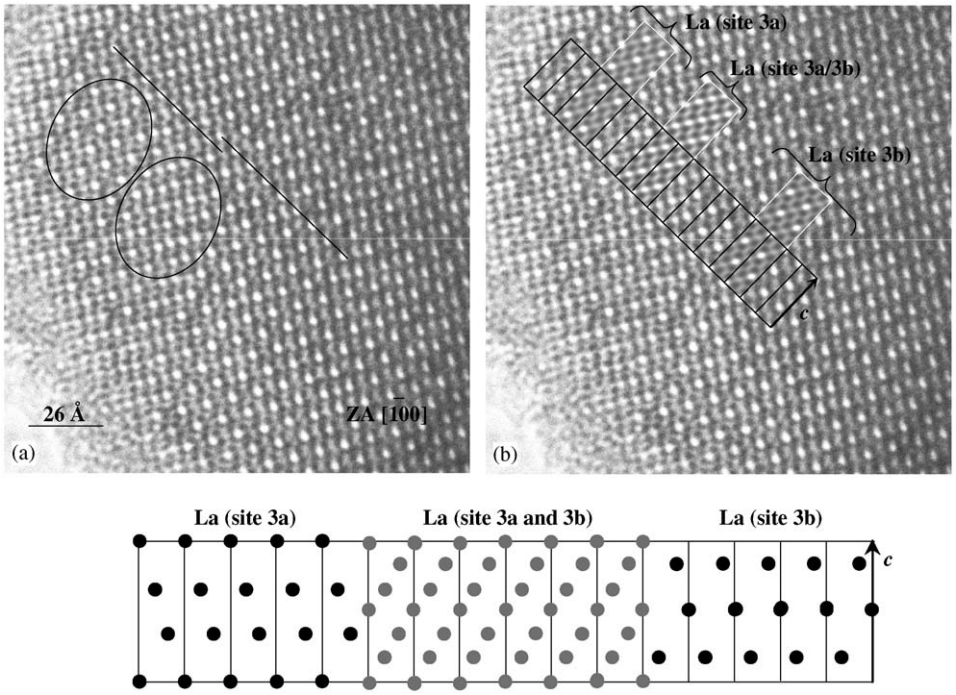

Fig. 5. (a) Experimental $[\bar{1}00]$ HREM images of $La_{1/3}Zr_2(PO_4)_3$. The circles show the two different contrasts observed while the black lines reveal a shift in the alignment of the white dots corresponding to a change in the local La^{3+}/vacancies ordering. In (b), several cells are drawn and three simulated images are inserted corresponding to different La^{3+} distributions: two La^{3+} cations in 3*a* site, one La^{3+} cations in 3*a* site and one La^{3+} cations in 3*b* site, two La^{3+} cations in 3*b* site. The same cells are drawn in the bottom of the figure showing the La^{3+} distribution modifications along the selected cells.

black lines show that the alignment of the white dots is clearly shifted.

In order to correlate the observed contrast with atomic columns, image simulation calculations are necessary. Thus, we need to propose an atomic model in the $R\bar{3}$ space group, group usually encountered for NASICON-type phase and in agreement with the extinction conditions obtained by the SAED study. If we accept the hypothesis

Table 2
Proposed model for $La_{1/3}Zr_2(PO_4)_3$ in a $R\bar{3}$ space group: atomic coordinates and selected interatomic distances (Å); ($a = 8.738$ Å, $c = 23.216$ Å)

Atoms	Site	x	y	z
Zr1	6*c*	0	0	0.145
Zr2	6*c*	0	0	0.647
P	18*f*	0.286	0.999	0.251
O1	18*f*	0.177	0.983	0.196
O2	18*f*	0.030	0.828	0.702
O3	18*f*	0.205	0.170	0.094
O4	18*f*	0.824	0.806	0.590
La1	3*a*	0	0	0
La2	3*b*	0	0	1/2

Zr octahedron	P tetrahedron	La polyhedron
Zr1–O1 : 3 × 2.011	P–O2 : 1.415	La1–O3 : 6 × 2.742
Zr1–O3 : 3 × 2.039	P–O3 : 1.512	
<Zr1–O> : 2.025	P–O4 : 1.516	La2–O4 : 6 × 2.645
Zr2–O2 : 3 × 2.086	P–O1 : 1.557	
Zr2–O4 : 3 × 2.093	<P–O> : 1.500	
<Zr2–O> : 2.089		

Table 3
Valence bond analysis for the model proposed for $La_{1/3}Zr_2(PO_4)_3$ in the $R\bar{3}$ space group using the Zachariasen law [8]

Atoms	O1	O2	O3	O4	Σ	Σexp
Zr1	3 × 0.81		3 × 0.75		4.68	4
Zr2		3 × 0.67		3 × 0.66	3.99	4
P	1.14	1.67	1.28	1.27	5.36	5
La1			6 × 0.21		1.26	3
La2				6 × 0.28	1.68	3
Σ	1.95	2.34	2.24	2.21		
Σexp	2	2	2	2		

that this $R\bar{3}$ form is directly related to the mother $P\bar{3}$ form, we can calculate the *x, y, z* coordinates of each atom assuming that its position is at the gravity center of the three atoms bounded nearly by a *R* translation (1/3, 2/3, 2/3 and 2/3, 1/3, 1/3). As an example, we can consider the Zr1 positions of the Table 2. In the $P\bar{3}$ space group, the zirconium atoms are located on six sites (two 2*c* sites and four 2*d* sites) [4], and the *R* translations (1/3, 2/3, 2/3 and 2/3, 1/3, 1/3), applied to Zr1 atom coordinates, allow to associate this position to Zr3 and Zr4:

Zr1 2*c* $(0, 0, \mathbf{0.1501})$

Zr3 2*d* $(1/3, 2/3, 0.8104) \equiv (1/3, 2/3, 2/3) + (0, 0, \mathbf{0.1437})$

Zr4 2*d* $(1/3, 2/3, 0.5241) \equiv (2/3, 1/3, 0.4759)$
$\equiv (2/3, 1/3, 1/3) + (0, 0, \mathbf{0.1426})$

The *z* coordinate of this hypothetic Zr1 atom in the $R\bar{3}$ space group can then be calculated easily:

$z = 1/3\ (0.1501 + 0.1437 + 0.1426) \approx 0.145$

With the same formalism, it is possible to deduce all the positional parameters of a complete hypothetical $R\bar{3}$ model given in Table 3, with the corresponding main interatomic distances. These values are in agreement with those usually encountered, leading to correct bond valence sums for all the atoms, except for the La^{3+} cations which are located in too large cages. As noticed above, a similar situation is observed for La^{3+} cations in $La_{1/3}Ti_2(PO_4)_3$ [9].

As we do not know the position of the La^{3+} cations in the cell, the image simulation calculations must be done at least for three hypotheses with the proposed model in the [$\bar{1}$00] ZA for a quadruple cell ($2 \times b$, $2 \times c$): in the first situation, the two La^{3+} cations are located in the 3a site (as in $La_{1/3}Ti_2(PO_4)_3$ [9]), leading to a 2/3 occupation factor (Fig. 6a); in the second one, the two La^{3+} cations are located in the 3*b* site, with 2/3 occupation factor (Fig. 6b); while in the third one, the La^{3+} cations are distributed on the two sites 3*a* and 3*b*, with an equal occupation factor of 1/3 (Fig. 6c). For a thickness close to 52 Å and a focus value of −80 nm (close to the Scherzer value), the white dots correspond to columns of La^{3+} empty sites for the three hypotheses (Fig. 6). The contrast evolution showed on the Fig. 5a can then be explained either by antiphase boundary with only one La^{3+} distribution (3*a* or 3*b*) or by two kinds of domains with distinct La^{3+} occupancy (3*a* and 3*b*): as revealed by the Figs. 6a and b, the simulated images for the 3*a* and 3*b* site occupations are the same and can be superposed by using a translation vector. In such conditions, we cannot choose between these two hypotheses. On Fig. 5b, we have represented on the HREM image, the simulations in the case of the domains hypothesis where several cells are drawn: on the top, if the localization of the white dots in the cell implies La^{3+} ions on the 3*a* sites, on the contrary, the 3*b* sites are occupied by the La^{3+} cations on the bottom. In the middle, the contrast observed can be explained by an intermediate situation with La^{3+} cations distributed over both available sites 3*a* and 3*b* or by a boundary between the two domains not parallel to the viewing direction. The local ordering of La^{3+} and vacancies in the selected cells of the Fig. 5b is drawn below in the case of the domains hypothesis.

4. Conclusion

During the TEM study (diffraction and high resolution) of the $La_{1/3}Zr_2(PO_4)_3$ NASICON-type compound of which the structure was determined by neutron and X-ray powder diffraction experiments, we have evidenced an irreversible structural change induced by the electron beam energy without modification of atomic content and cell size. This transformation is followed on SAED patterns along [001] and [100] ZA and reveals a rapid disappearance of the *h k l* spots forbidden in an *R* mode, while no information on the original mother form $P\bar{3}$ can be obtained because the crystallite structure changes as soon as it is illuminated. It

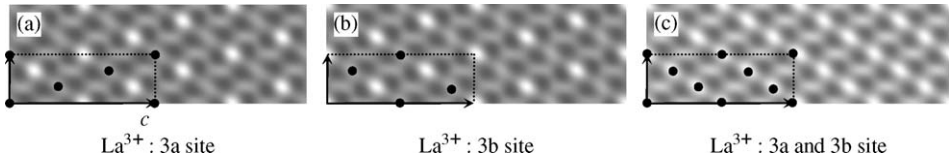

Fig. 6. Simulated $[\bar{1}00]$ images calculated with the proposed $R\bar{3}$ model (thickness and focus value, respectively, close to 52 Å and −80 nm) for a quadruple cell with different La^{3+} locations showing that the white spots can be directly correlated with La^{3+} empty sites. In (a), the 3*a* site is occupied by 2/3 La^{3+} and 1/3 vacancies; in (b), the 3*b* site is occupied by 2/3 La^{3+} and 1/3 vacancies; in (c), the sites 3*a* and 3*b* are both occupied by 1/3 La^{3+} and 2/3 vacancies.

is worthy to note that this structural reorganization (P - - - $\rightarrow P$ - c - $\rightarrow R$ - - -) implies the displacement of the two La^{3+} ions in a preserved $[Zr_2(PO_4)_3]^-$ NASICON network. HREM image confirms the $R\bar{3}$ calculated $[Zr_2(PO_4)_3]^-$ network and excludes a statistic repartition of the two La^{3+} ions over the 3*a* and 3*b* available sites. The ability of La^{3+} ions to move is in good agreement with the ionic conductivity (4.09×10^{-7} S cm^{-1} at 700 °C) observed for $La_{1/3}Zr_2(PO_4)_3$. Thermal X-ray diffraction experiments show subtle and slow modifications confirming the La^{3+} displacements with a change of the space group from $P\bar{3}$ to $P\bar{3}c1$ at 1000 °C while no transition is revealed by DTA analysis. All these results will be published in a next coming paper. Finally, since the La^{3+} is the larger lanthanon ion, it would be very interesting to study the other $RE_{1/3}Zr_2(PO_4)_3$ compounds which are also found to be trivalent cationic solid electrolytes.

References

[1] (a) M. Catti, S. Stramare, R. Ibberson, Solid State Ion. 123 (1999) 173;
(b) M. Catti, S. Stramare, Solid State Ion. 136–137 (2000) 489;
(c) A. Aatiq, M. Ménétrier, L. Croguennec, E. Suard, C. Delmas, J. Mater. Chem. 12 (2002) 2971;
(d) J.E. Iglesias, C. Pecharroman, Solid State Ion. 112 (1998) 309;
(e) S. Senbhagaraman, A.M. Umarji, J. Solid State Chem. 85 (1990) 169;
(f) D.A. Woodcock, P. Lightfoot, R.I. Smith, J. Mater. Chem. 9 (1999) 2631;
(g) A. Mouline, M. Alami, R. Brochu, R. Olazcuaga, C. Parent, G. Le Flem, Mater. Res. Bull. 35 (2000) 899.
[2] M. Sljukic, B. Matkovic, B. Prodic, S. Scavnicar, Croatia Chem. Acta 39 (1967) 145.
[3] (a) S. Tamura, N. Imanaka, G. Adachi, Solid State Ion. 136-137 (2000) 423;
(b) S. Tamura, N. Imanaka, G. Adachi, J. Mater. Sci. Lett. 20 (2001) 2123;
(c) S. Tamura, N. Imanaka, M. Kamikawa, G. Adachi, Sens. Actuat. B 73 (2001) 205;
(d) S. Tamura, N. Imanaka, G. Adachi, J. Alloys Compd. 323–324 (2001) 540;
(e) N. Imanaka, G. Adachi, J. Alloys Compd. 344 (2002) 137;
(f) S. Tamura, N. Imanaka, G. Adachi, Solid State Ion. 154–155 (2002) 767;
(g) S. Tamura, N. Imanaka, G. Adachi, Recent Res. Dev. Solid State Ion. 1 (2003) 189.
[4] M. Barre, M.P. Crosnier-Lopez, F. Le Berre, J. Emery, E. Suard, J.L. Fourquet, Chem. Mater. 17 (2005) 6605.
[5] (a) M.P. Pechini, US Patent no. 3. 330 (1967) 697;
(b) M. Kakihana, J. Sol–Gel Sci. Technol. 6 (1996) 7.
[6] P.A. Stadelman, Ultramicroscopy 21 (1987) 131.
[7] R.D. Shannon, Acta Crystallogr. A 32 (1976) 751.
[8] N.E. Brese, M. O'Keeffe, Acta Crystallogr. B 47 (1991) 192.
[9] P. Lightfoot, D.A. Woodcock, J.D. Jorgensen, S. Short, Int. J. Inorg. Mater. 1 (1999) 53.